Journal of Magnetic Resonance **153,** 227–237 (2001)
doi:10.1006/jmre.2001.2446, available online at http://www.idealibrary.com on IDEAL®

Bond-Shift Rearrangement in Solid $Li_3P_7(Monoglyme)_3$: A ^{31}P MAS NMR Study

Christian Jäger,* Detlef Reichert,† Herbert Zimmermann,‡ Tapas Sen,§ Raphy Poupko,§ and Zeev Luz§

*Institut für Optik und Quantenelectronik, Friedrich-Schiller-Universität Jena, Max-Wien-Platz 1, D-07743 Jena, Germany; †Fachbereich Physik, Martin-Luther-Universität, Halle-Wittenberg, 06108 Halle, Germany; ‡A.G. Molekülkristalle, Max-Planck-Institut für Medizinische Forschung, Jahnstrasse 29, 69120 Heidelberg, Germany; and §Weizmann Institute of Science, Rehovot 76100, Israel

Received April 27, 2001; revised September 17, 2001; published online November 7, 2001

The ^{31}P MAS NMR spectrum of solid $Li_3P_7(monoglyme)_3$ has been reinvestigated over a wide temperature range (−70 to +77°C) and under conditions of better resolution (Larmor frequency of 162 MHz and spinning rate of ∼30 kHz) than previously measured (121 MHz and 13 kHz). At low temperatures three spinning sideband (ssb) manifolds are observed: a singlet (centered at −45 ppm relative to 85% H_3PO_4) due to the apical atom (A) of the P_7-cage trianion; a 1:1:1 triplet (at −110, −117, and −124.5 ppm) due to the negatively charged equatorial (E) atoms, and a one to two doublet (at −161 and −168.5 ppm) due to the basal (B) atoms. These results are consistent with the P_7 cage having nearly, but not perfect, C_{3v} symmetry. The compound appears to be well ordered in the solid state with very little structural dispersity. On heating, the NMR lines broaden and eventually coalesce into a single ssb manifold. This behavior is ascribed to bond-shift rearrangement similar to the Cope rearrangement in bullvalene. A MAS 2D exchange experiment and a quantitative analysis of the 1D NMR lineshapes indicate that, unlike in solution where the rearrangement involves a single bond shift at a time, in the solid the process involves a succession of two bond shifts: The first leads to an intermediate species in which the rearranged P_7 cage is inverted, while in the subsequent step a second bond shift takes place that also restores the original orientation of the cage in the lattice. The overall effect of the double bond shift is equivalent to cyclic permutation of the phosphorus atoms within the five member rings of the P_7-cage. The quantitative analysis of the dynamic lineshapes shows that this cyclic permutation proceeds at a different rate in one ring (k_a^1) than in the other two ($k_a^{2,3}$). The kinetic parameters for these processes are $E_a^1 = 18.7$ kJ/mol, $E_a^{2,3} = 58.0$ kJ/mol, $k_a^1(17°C) = k_a^{2,3}(17°C) = 10^4\ s^{-1}$. No indications for independent threefold molecular jumps of the P_7 cage were found.

1. INTRODUCTION

In a recent publication Sen *et al.* (*1*) have described and analyzed the magic angle spinning (MAS) ^{31}P NMR spectra of solid $Li_3P_7(monoglyme)_3$ (henceforth we refer to the quoted paper as I and to the compound as $Li_3P_7(mg)_3$). The results revealed the presence of an interesting rearrangement process, but its mechanism could not be fully analyzed because of poor spectral resolution. In the present work we revisit this system using a highly improved experimental setup, which provided much better resolved spectra that could quantitatively be analyzed. This analysis yielded a complete description of the pathway of the rearrangement reaction.

The $Li_3P_7(mg)_3$ compound belongs to the homologous series (*2*) of salts containing the P_7-cage trianion, shown in the diagrams of Fig. 1. This cage consists of seven phosphorus atoms linked together into a basket shape of nearly C_{3v} symmetry, with one apical (A), three negatively charged equatorial (E), and three basal (B) atoms. The negative charges on the E atoms are compensated by three Li^+ cations, which are ligated by the bidentate ligand, monoglyme (CH_3–OCH_2CH_2O–CH_3). The compound is sensitive to air and humidity and is soluble in a number of organic solvents, but does not crystallize well from solutions. It was, in fact, claimed to be "X-ray amorphous" (*3*) and therefore no direct structural information on $Li_3P_7(mg)_3$ is available. On the other hand, the NMR results, to be described below, indicate that $Li_3P_7(mg)_3$ forms a well-ordered solid with, at most very little, structural dispersity. We therefore assume that its structure is similar to that of the $Li_3P_7(tmeda)_3$ homologue (tmeda = tetramethylethylenediamine), whose structure has been determined by X-ray (*4*). On this basis, we assume that the Li cations are each coordinated, pseudo tetrahedrally, to two E phosphorus atoms and two oxygens of a monoglyme ligand. They are located, approximately, on the bisectors of the equatorial triangle and form a "belt" around the P_7 cage, as shown schematically in Fig. 1A. These assumptions have no consequences on the conclusions derived below. The ^{31}P MAS spectra, reported in I, exhibit, at low temperatures, three sets of spinning sideband (ssb) manifolds. On the basis of earlier solution studies (*5–7*) they were identified as being due to the apical (centered at −43 ppm relative to 85% H_3PO_4), equatorial (−119 ppm), and basal (−167 ppm) phosphorus atoms. The equatorial signals exhibited a nonsymmetric triplet structure which was interpreted in I as due to the residual dipolar splitting (*8*) between the phosphorus E atoms and the quadrupolar Li nuclei.

Above about −40°C line broadening was found to sets in (*1*), leading to coalescence and eventually, above room temperature,

1090-7807/01 $35.00

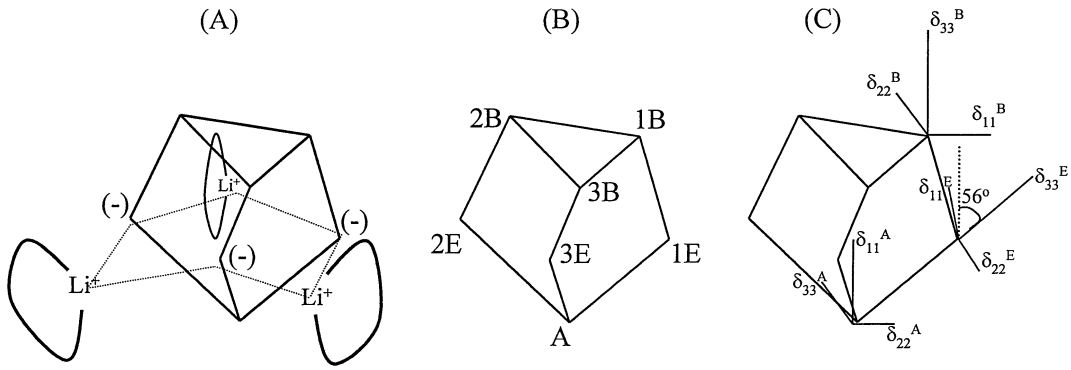

FIG. 1. Structure and labeling of the P_7 cage in solid $Li_3P_7(mg)_3$. (A) Structure showing the positions of the Li^+ ions. The loops represent the bidentate monoglyme ligands and the − signs represent the negative charges on the equatorial phosphorus atoms. (B) The labeling of the phosphorus sites in the P_7 cage. A, E, and B stand for apical, equatorial, and basal atoms and the numbers label the three wings of the cage. (C) The orientations of the principal axes systems (PAS) of the anisotropic chemical-shift tensors of atoms 1B, 1E, and A. The orientations associated with δ_{11}^A and δ_{33}^B are parallel to the pseudo C_3 axis of the P_7 cage, δ_{33}^E is tilted 56° from this axis, and the components δ_{11}^B and δ_{22}^E lie in the plane of the wing defined by the atoms 1B, 1E, and A. The PAS of the other E and B atoms are obtained from those of 1E and 1B by appropriate threefold rotation.

to a single ssb manifold. This effect is clearly due to a bond-shift rearrangement similar to the well-known Cope rearrangement in bullvalene (*9–11*).

For the P_7 cage the process involves the displacement of electrons from two of the negatively charged equatorial atoms to the nearby basal atoms (while in bullvalene a similar displacement of electrons occurs, but involving double bonds). See Scheme A. The bond-shift process in the P_7 cage was extensively studied in solutions of $Li_3P_7(mg)_3$ by Baudler *et al.* (*5–7*) and in I it was first shown to occur also in the solid state. The quality of the MAS spectra in the latter work was, however, not sufficient for a comprehensive analysis of the lineshapes in terms of the detailed pathways of the bond-shift process. Also under the experimental conditions of I (relatively low spinning rate) the lineshapes were not very sensitive to the assumed mechanism of the rearrangement process. Dynamic spectra were simulated for a wide range of pathways but none fitted satisfactorily the experimental results. For lack of alternative conclusions a concerted single bond-shift/reorientation mechanism, analogous to that found in solid bullvalene (*10–12*) was finally adopted and kinetic parameters for this mechanism were estimated from the dynamic lineshapes (*1*).

In the present work we reinvestigate the $Li_3P_7(mg)_3$ system by ^{31}P MAS NMR under significantly improved experimental conditions. In particular, we use a higher magnetic field, corresponding to a ^{31}P Larmor frequency of 162 MHz, and apply a considerably faster spinning of almost 30 kHz (compared to 121 MHz and 13 kHz, respectively, in I). These improved conditions resulted not only in a better signal sensitivity, but also in well-featured dynamic lineshapes that could readily be used to discriminate between different dynamic pathways. We have also performed 2D exchange experiments, the results of which are in full agreement with those derived from fitting the dynamic 1D spectra. The main conclusion of I, i.e., that the process responsible for the dynamic line broadening of the ^{31}P NMR spectra involves a bond-shift rearrangement, still holds. However, the details of the reaction pathway turned out to be quite different. Rather than a single bond-shift in concert with molecular reorientation, as suggested in I, analysis of the results shows that in solid $Li_3P_7(mg)_3$ the reaction pathway involves two consecutive bond-shifts, with an inverted P_7 cage as intermediate. This two-step bond-shift process corresponds to a cyclic permutation of the phosphorus atoms within one of the five-member rings (five rings) of the P_7 cage. The NMR spectra indicate that the symmetry of the P_7 cage in solid $Li_3P_7(mg)_3$ is almost, but not perfectly, C_{3v}, as also found by X-ray for the P_7 cage in the homologous $Li_3P_7(tmeda)_3$ compound. The lack of perfect C_{3v} symmetry is reflected in the presence of different permutation rates for the different five rings in the P_7 cage.

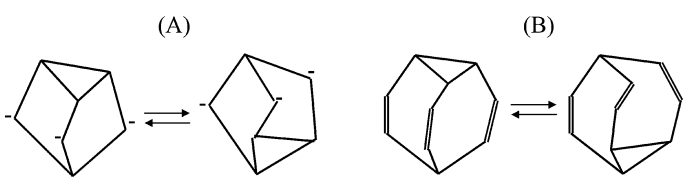

SCHEME A. Bond-shift rearrangement in the P_7 cage (A) and in bullvalene (B).

2. EXPERIMENTAL

$Li_3P_7(mg)_3$ was obtained from ACROS ORGANICS and was used without further treatment. This sample came from a much purer batch than used in I. In particular its ^{31}P MAS NMR spectrum did not show the vexing impurity peak at 64 ppm observed in the previous work (*1*). The samples for the MAS NMR measurements were prepared by packing the compound into 2.5-mm rotors in a glovebox flushed with dry argon. The rotors

were sealed with ceramic caps and kept under argon before use. The NMR measurements were performed on a Bruker AMX400 spectrometer operating at a ^{31}P frequency of 162 MHz. The temperature calibration was done for a number of spinning rates using the ^{207}Pb chemical shift in a reference $Pb(NO_3)_2$ sample (*13*). However, for technical reasons, the calibration was carried out only several weeks after the measurements. This delay may have caused a relatively large systematic (constant) error in the reported temperatures, of up to $\pm$(5–10)°C. This uncertainty does not affect any of the conclusions related to the mechanistic analysis of the results and only slightly affects the derived activation parameters. The simulations of the dynamic MAS NMR lineshapes were performed using the Floquet method (*14, 15*) as explained in I. A total of 13 Floquet states for each phosphorus atom were included in the calculations, resulting in 91 × 91 Floquet matrices, from which the dynamic lineshapes were computed.

3. RESULTS AND DISCUSSION

3.1. The Low-Temperature Spectrum

Most MAS measurements reported in the present paper were run at a spinning rate of almost 30 kHz. However, because of frictional heating, it was not possible to cool the sample below about −60°C at this spinning rate, so that at lower temperatures slower spinning had to be used. Such a spectrum is shown in the top trace of Fig. 2. It was recorded at −70°C with a spinning rate of 16.4 kHz. At this temperature range there is essentially no exchange broadening and, for the particular spinning rate chosen, there is no overlap between the various ssb. The center bands, as well as the first and, for most peaks also, higher order ssb are observed. They were identified as such by recording additional spectra at slightly different spinning rates. The bands due to the apical (A), equatorial (E), and basal (B) atoms are well resolved and can readily be identified. For the apical atoms, only weak first order (and no higher order) ssb are observed, because of their relatively small chemical shift anisotropy. Evidently, while peak A is a relatively sharp singlet, the equatorial band consists of a 1 : 1 : 1, nearly equally spaced (∼1.1 kHz) triplet and the basal signal exhibits an unresolved 1 : 2 doublet. Similar although less resolved splittings were also observed in I. There, the splitting was ascribed to the residual dipolar interaction between the phosphorus ($I = \frac{1}{2}$) and the quadrupolar ^{6}Li/^{7}Li nuclei ($S = \frac{3}{2}$). This interpretation does not seem to hold, however. An estimate of the expected splitting, Δ, due to this effect can be calculated from the expression (*8*)

$$\Delta \sim \chi D/\nu_S, \qquad [1]$$

where χ is the quadrupolar coupling constant of the S spins, D is the dipolar interaction, and ν_S is the Larmor frequency of the S spins. Considering the equatorial atoms and inserting reasonable values for the various parameters (χ(Li) ∼ 50 kHz,[1] D(Li-P) ∼ 2 kHz) yields Δ ∼1 Hz, which is much too small to account for the observed splitting. Also, if the splitting were indeed of such a second-order dipolar origin, it should have been smaller in the present spectrum, which was recorded at a higher magnetic field than in I. In fact, the splitting is somewhat larger. The observed splitting is also not consistent (much too large) to be ascribed to scalar couplings between the phosphorus nuclei in the P_7 cage. These interactions were measured in solution (*6*) and found to be ∼400 Hz and less.

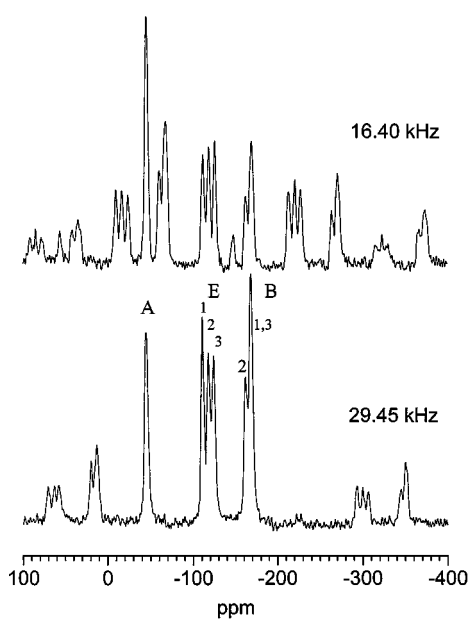

FIG. 2. Experimental ^{31}P MAS NMR spectra of solid $Li_3P_7(mg)_3$. Top: Recorded at −70°C (spinning rate, 16.4 kHz; number of scans, 4; recycle time, 240 s; line broadening parameter, 50 Hz). Bottom: Recorded at −60°C (spinning rate, 29.45 kHz; number of scans, 8; recycle time, 90 s; line broadening parameter, 50 Hz). The assignments of the center bands are indicated on the bottom trace.

We are thus led to conclude that the splittings of the E and B bands reflect the inequivalence of the three equatorial and three basal phosphorus atoms and are due to slight differences between their isotropic chemical shifts. This implies that the P_7 cage lacks perfect C_{3v} (or even C_{2v}) symmetry. At the same time, the well-resolved triplet structure of the E band indicates that the system (even though perhaps not crystalline) is ordered and that all cages have essentially the same packing environment with at most very little structural dispersity. The structure of the basal signal (1 : 2 doublet) can be explained in terms of one separate and two, almost overlapping, peaks. As another example we show in the bottom trace of Fig. 2 a spectrum measured at −60°C and a spinning frequency of 29.45 kHz. It may be seen that some exchange broadening has already set in at this temperature, but the peaks are still well resolved. These and several other low-temperature spectra were subject to a Herzfeld–Berger type analysis (*16*), yielding the chemical shift tensors summarized in Table 1. Also included in the table are the exchange independent linewidths of the various peaks, obtained by best fitting the results to calculated spectra. The anisotropic parts of the chemical

TABLE 1
Chemical Shift Tensors and Linewidth Parameters for the Phosphorus Nuclei in Solid $Li_3P_7(mg)_3$[a]

	A	1E	2E	3E	1B	2B	3B
δ_{iso}[b]	−45	−110/−108	−117/−119	−124.5/−123	−168/−166	−161/−159	−169/−174
δ_{11}	126	249	249	249	255	255	255
δ_{22}	−63	−21	−21	−21	45	45	45
δ_{33}	−63	−228	−228	−228	−300	−300	−300
$\Delta_{\frac{1}{2}}$[c]	320	320	320	320	370	370	370

[a] The isotropic chemical shifts are in ppm relative to 85% H_3PO_4. The δ_{ii} are the principal values of the anisotropic chemical shift tensors in the corresponding principal axis system, so that $\delta_{11} + \delta_{22} + \delta_{33} = 0$. The principal directions for 1E, 1B, and A are shown in Fig. 1C. Those for the other E and B atoms are related to the latter by appropriate threefold rotations.

[b] The double entries indicate the range of the isotropic chemical shifts used to optimize the fit of the dynamic data. The left and right entries correspond to the −70 and −4°C spectra, respectively. Within this range δ_{iso} was changed linearly with the temperature. Above this range no further adjustment in δ_{iso} was made.

[c] Half width at half maximum height, in Hz, as obtained by fitting the low-temperature spectra.

shift tensors are essentially identical to those calculated in I, but here we have also identified the isotropic chemical shift of the different E and B atoms. The determination and assignment of the isotropic chemical shifts of the three B atoms are based on the analysis of the dynamic spectra, to be described in the next section. For this analysis we needed the principal directions for the anisotropic chemical shift tensors. These we have adopted from I, where they were obtained from quantum mechanical calculations. They are reproduced in Fig. 1C.

3.2. The Dynamic Spectra—Failure of the Single Bond-Shift Mechanism

On the left hand side of Fig. 3 are shown experimental dynamic MAS spectra of $Li_3P_7(mg)_3$ (spinning rate, 29.45 kHz) over the temperature range −39 to +77°C. Over this temperature range the spectral peaks first broaden, then coalesce into a single ssb manifold and eventually sharpen again. This behavior can only be explained in terms of a bond-shift rearrangement mechanism that leads to complete scrambling of all sites in the P_7 cage. Since, however, $Li_3P_7(mg)_3$ is ordered, the reaction must be such that the orientation of the cage before and after the bond shift remains the same. To meet this requirement it was assumed in I, in analogy with the situation in solid bullvalene (*10–12, 17*), that the rearrangement involves two concerted steps: a chemical rearrangement and an overall molecular reorientation that restores the P_7 cage to its original orientation. The process can be described as in Scheme B1. The first step in this scheme represents the chemical rearrangement, which

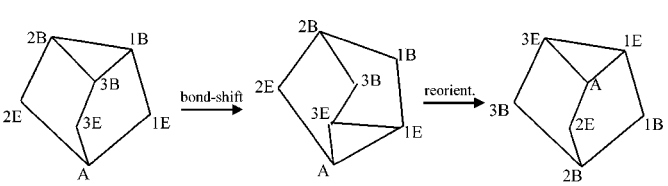

SCHEME B1. Single bond-shift/reorientation mechanism. Molecular structure representation.

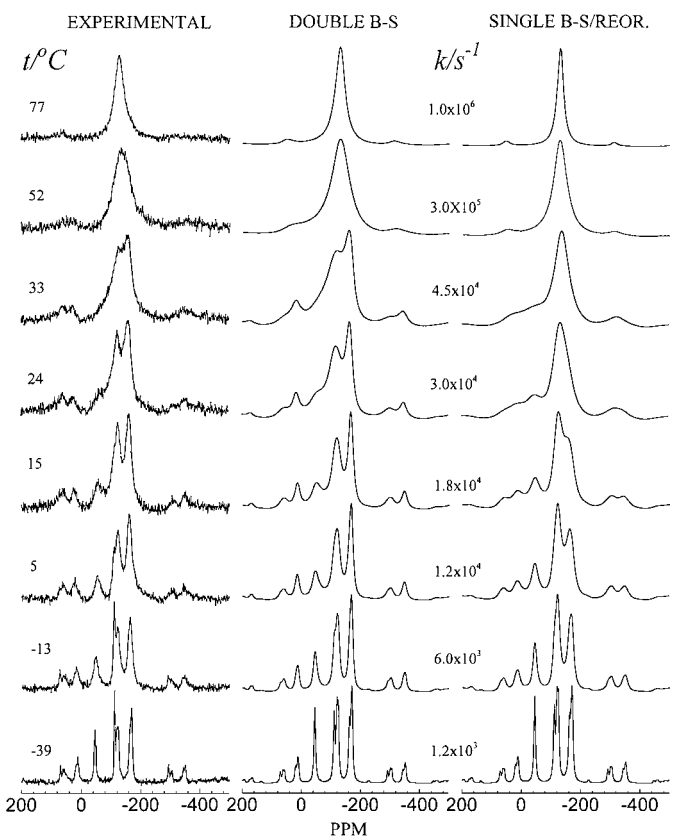

FIG. 3. Dynamic ^{31}P MAS NMR spectra of solid $Li_3P_7(mg)_3$ (spinning frequency, 29.45 kHz). Left column: Experimental spectra recorded at the indicated temperatures. Recycle time, 90 s (except for the −39°C trace for which it was 240 s). The number of scans was 16 for the dynamically broadened traces (5 to 52°C) and 4 or 8 for, respectively, the low- and high-temperature spectra (−39, −13, and 77°C). The line-broadening parameter was 20 Hz. Center column: Simulated dynamic spectra for the double bone-shift mechanism, assuming $k_d^1 = k_d^2 = k_d^3 = \frac{1}{3}k_d$ (Eq. [8]), calculated using the parameters of Table 1 (and Fig. 1) and the indicated rate constants. Right column: As in the center column for the single bond-shift/reorientation mechanism (Eq. [3]). The rates k correspond to k_d for the second column and to k_s for the third one.

$$\begin{bmatrix} 1B & 2B & 3B \\ 1E & 2E & 3E \\ & A & \end{bmatrix} \xrightarrow{\text{bond-shift}} \begin{bmatrix} & 2B & \\ 1B & 2E & 3B \\ 1E & A & 3E \end{bmatrix} \xrightarrow{\text{reorient.}} \begin{bmatrix} 1E & 3E & A \\ 1B & 3B & 2E \\ & 2B & \end{bmatrix}$$

SCHEME B2. Single bond-shift/reorientation mechanism. 3×3 chart representation.

consists of the cleavage of one of the iB–jB bonds (1B–3B in the example depicted in Scheme B1) and the formation of the corresponding iE–jE bond (1E–3E). Here the coefficients i and j label the "wings" of the P_7 cage. In concert with the rearrangement the P_7 cage reorients into its original orientation in the lattice as shown by the second step of Scheme B1. To facilitate the discussion we rewrite this scheme in a more concise and easy to follow way. Accordingly we represent the P_7 cages by 3×3 charts, so that the above scheme acquires the form shown in Scheme B2. In each chart the apical atom appears alone in the row, next are the equatorial atoms, and then the basal ones. For comparison with the molecular structure a clockwise rotation about a C_3 axis pointing upward is assumed. As in Scheme B1, the first step represents the bond-shift rearrangement, obtained by shifting "upward" the string of atoms comprising the wing that remains intact (does not participate in the bond shift)—in the present case this is the center column A–2E–2B. The second step represents the realignment of the cage to its original orientation in the lattice. In this chart representation the second stage (reorientation) requires the interchange of atoms of two of the wings in order to keep the sense of rotation as in the structural formulae. Note that in these schemes the symbols of the original structure or chart (the leftmost in each scheme) have double meanings; they label both the molecular site and the atom in the site. For example, A is the symbol of the apical site, as well as of the atom in this site. In the other charts the sites are not indicated and the symbols apply to the (original) names of the atoms. Thus, in the right chart of Scheme B2, the atom originally named A is now in site 3B, etc. Comparing the positions of the various atoms in the first and last charts of Schemes B1 and B2 yields the following exchange matrix

$$R = kK = k \begin{pmatrix} -1 & 0 & 0 & 0 & 0 & 1 & 0 \\ 0 & -1 & 0 & 0 & 1 & 0 & 0 \\ 0 & 0 & -1 & 0 & 0 & 0 & 1 \\ 0 & 0 & 1 & -1 & 0 & 0 & 0 \\ 0 & 1 & 0 & 0 & -1 & 0 & 0 \\ 0 & 0 & 0 & 1 & 0 & -1 & 0 \\ 1 & 0 & 0 & 0 & 0 & 0 & -1 \end{pmatrix}. \quad [2]$$

In this matrix the rows and columns are labeled according to the order, A, 1E, 2E, 3E, 1B, 2B, 3B; k is the rate constant for the reaction; and K is the exchange probability matrix with K_{ij} the probability that if a rearrangement takes place it will result in a transition from site j to site i.

The exchange matrix, Eq. [2], represents one out of nine possible bond-shift/reorientation pathways. This is so because the bond shift may involve each of the three pairs iB–jB/iE–jE of bond cleavage/formation, and each rearrangement may end up in three different final orientations of the cage in the lattice. In the example above where the bond shift involves the 1B–3B/1E–3E pair, two more final orientations of the P_7 cage are possible (obtained by threefold rotations of the end result in the above scheme), namely,

$$\begin{bmatrix} A & 1E & 3E \\ 2E & 1B & 3B \\ & 2B & \end{bmatrix} \quad \text{and} \quad \begin{bmatrix} 3E & A & 1E \\ 3B & 2E & 1B \\ & 2B & \end{bmatrix}.$$

The other six end results, for a single bond-shift/reorientation process, are

$$\begin{bmatrix} 1B & 2B & 3B \\ 1E & 2E & 3E \\ & A & \end{bmatrix} \xrightarrow{\text{bond-shift}} \begin{bmatrix} & 3B & \\ 1B & 2B & 3E \\ 1E & 2E & A \end{bmatrix} \xrightarrow{\text{reorient.}} \begin{bmatrix} 1E & A & 2E \\ 1B & 3E & 2B \\ & 3B & \end{bmatrix}$$

$$\text{or} \quad \begin{bmatrix} 2E & 1E & A \\ 2B & 1B & 3E \\ & 3B & \end{bmatrix} \quad \text{or} \quad \begin{bmatrix} A & 2E & 1E \\ 3E & 2B & 1B \\ & 3B & \end{bmatrix}$$

for the 1B–2B/1E–2E rearrangement, and

$$\begin{bmatrix} 1B & 2B & 3B \\ 1E & 2E & 3E \\ & A & \end{bmatrix} \xrightarrow{\text{bond-shift}} \begin{bmatrix} & 1B & \\ 1E & 2B & 3B \\ A & 2E & 3E \end{bmatrix} \xrightarrow{\text{reorient.}} \begin{bmatrix} A & 3E & 2E \\ 1E & 3B & 2B \\ & 1B & \end{bmatrix}$$

$$\text{or} \quad \begin{bmatrix} 2E & A & 3E \\ 2B & 1E & 3B \\ & 1B & \end{bmatrix} \quad \text{or} \quad \begin{bmatrix} 3E & 2E & A \\ 3B & 2B & 1E \\ & 1B & \end{bmatrix}$$

for the 2B–3B/2E–3E rearrangement, where the charts separated by "or" are related to each other by threefold rotations. In I it was assumed that all nine pathways have equal probabilities (identical rates constants), resulting in an overall exchange matrix of

the form,

$$R_s = k_s K_s = k_s \frac{1}{9} \begin{pmatrix} -9 & 0 & 0 & 0 & 3 & 3 & 3 \\ 0 & -8 & 1 & 1 & 2 & 2 & 2 \\ 0 & 1 & -8 & 1 & 2 & 2 & 2 \\ 0 & 1 & 1 & -8 & 2 & 2 & 2 \\ 3 & 2 & 2 & 2 & -9 & 0 & 0 \\ 3 & 2 & 2 & 2 & 0 & -9 & 0 \\ 3 & 2 & 2 & 2 & 0 & 0 & -9 \end{pmatrix}, \quad [3]$$

where $k_s = 9k$ and the subscript s stands for single bond-shift rearrangement. Repeated exchanges of this type eventually generate all the $7! = 5040$ possible permutations of the phosphorus atoms in the P_7 cage. In the fast exchange limit this renders all the phosphorus atoms magnetically equivalent, resulting in a single ssb manifold in the MAS spectrum.

Using Eq. [3] we have simulated the spectra shown in the right column of Fig. 3. Although, in general, these spectra reproduce the main features of the experimental results, especially the coalescence into a single ssb manifold, in details they do not match the experimental lineshapes. In particular, the calculated relative broadening of the E and B bands deviate considerably from that observed in the experiment. Clearly a different pathway (or several pathways) must be assumed for a faithful simulation of the experiments.

To aid in the search for alternative pathways we have performed a rotor-synchronized 2D MAS exchange experiment (*18*) on the $Li_3P_7(mg)_3$ sample at -35°C with a mixing time of $\tau = 2$ ms and a spinning rate of 25 kHz. The result is displayed as a magnitude spectrum on the right-hand side of Fig. 4. At -35°C there is already some line broadening and the fine structure of the E and B bands is partially blurred. We therefore confine our discussion to exchange between the main groups of nuclei in the P_7 cage, i.e., the A, E, and B phosphorus atoms, disregarding the fine structure and the ssb. Referring to Fig. 4 we readily notice cross peaks linking the E/B and A/E pairs, but no such cross peaks between A and B. This result is completely inconsistent with any single bond-shift mechanism. To see why, we contract the (7×7) exchange matrix for R_s (Eq. [3]) by grouping together sites belonging to the same type of atoms. The result is

$$R_s^* = k_s K_s^* = k_s \begin{pmatrix} -1 & 0 & \frac{1}{3} \\ 0 & -\frac{2}{3} & \frac{2}{3} \\ 1 & \frac{2}{3} & -1 \end{pmatrix}, \quad [4]$$

where the columns and rows are now labeled in the order A, E, B. To compare with the experimental 2D spectrum (right-hand side of Fig. 4) we recall that for short mixing times ($k_s\tau < 1$) the intensities of the i, j cross peaks are proportional to $R_{ij}P_j^o$, where P_j^o is the fractional equilibrium population of site j (in our case 1/7, 3/7, and 3/7, for the A, E, and B types of atoms, respectively). This matrix thus predicts that in a 2D exchange

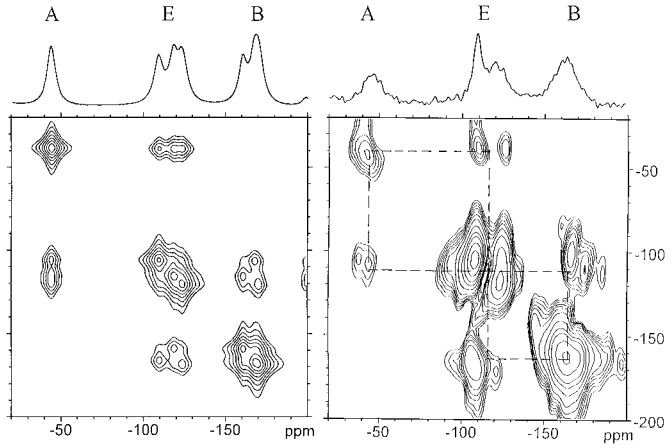

FIG. 4. Two-dimensional ^{31}P (magnitude) MAS exchange spectra of solid $Li_3P_7(mg)_3$ at a spinning rate of 25 kHz. Only the center bands and corresponding 1D projections are shown. Right: Experimental spectrum recorded at -35°C with a mixing time of $\tau = 2$ ms, 64 t_1 increments, spaced 10 μs apart, with a minimum phase cycle of 8 scans per increment, and a recycle time of 60 s. The number of acquisition points in t_2 was 1024 with a dwell time of 2.5 μs. The dashed lines indicate the connectivity of the cross peaks. Left, simulated spectrum for the double bond-shift mechanism, Eq. [8], with $k_d\tau = 1$.

experiment cross peaks linking the pairs A/B and E/B would appear, but, to first order in the mixing time, no such cross peaks are expected between A and E. This is, in fact, the type of 2D spectrum obtained by Baudler *et al.* (*7*) for the bond-shift rearrangement in a THF solution of $Li_3P_7(mg)_3$. The experimental 2D spectrum in Fig. 4 is, however, quite different. We therefore rule out single bond-shift pathways as the mechanisms responsible for the dynamic lineshapes in solid $Li_3P_7(mg)_3$.

3.3. The Double Bond-Shift Mechanism

We thus seek an alternative mechanism to the bond-shift/reorientation pathway, which will be consistent with the 2D exchange result and reproduce well the experimental 1D spectra. Such a mechanism turns out to be a process involving a sequence of two consecutive bond shifts. The first step is a bond-shift resulting in an inverted P_7 cage, as in Schemes B1, B2 above. It is then immediately followed by a second bond shift, rather than a reorientation step, that further permutes the atoms in the cage and at the same time restores it to its original orientation in the lattice. As for the single bond shift, there are several pathways for the double bond-shift mechanism. One such pathway is shown in Scheme C1. In this scheme, the first

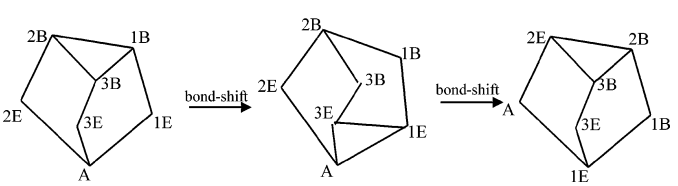

SCHEME C1. Double bond-shift mechanism. Molecular structure representation.

$$\begin{bmatrix} 1B & 2B & 3B \\ 1E & 2E & 3E \\ & A & \end{bmatrix} \xrightarrow{\text{bond-shift}} \begin{bmatrix} & 2B & \\ 1B & 2E & 3B \\ 1E & A & 3E \end{bmatrix}$$

$$\xrightarrow{\text{bond-shift}} \begin{bmatrix} 2B & 2E & 3B \\ 1B & A & 3E \\ & 1E & \end{bmatrix}$$

SCHEME C2. Double bond-shift mechanism 3 × 3 chart representation.

and second bond shifts are, respectively, of the type 3B–1B/3E–1E and A–3E/2E–3B, where the symbols refer to the names of the atoms. In terms of the chart representation this pathway acquires the form shown in Scheme C2. In this scheme, the first bond shift is represented by "pushing up" the center column, while the second bond shift corresponds to "pushing down" the left column. In a similar way one can imagine a rearrangement involving pushing up the center column, followed by pushing down the right column. Clearly, pushing up and down the same column do not result in rearrangement, so that for each upward shift there are two downward shifts, i.e., all together six distinct double bond-shift pathways.

A convenient way to enumerate these pathways is in terms of the corresponding permutation diagrams. Inspection of the double bond-shift Schemes C1 and C2 shows that they correspond to a cyclic permutation of the phosphorus atoms around one of the five rings of the P_7 cage, while the two remaining atoms remain in their original molecular sites. For the example in Schemes C1 and C2, the permutation can be described as (*19*)

$$(1B, 1E, A, 2E, 2B)(3B)(3E).$$

There is, of course, also the pathway corresponding to the reverse permutation (pushing up the left column and down the center one),

$$(1B, 2B, 2E, A, 1E)(3B)(3E).$$

By the principle of microscopic reversibility (*20*), these two pathways must have identical rates. We therefore lump them together into a single, symmetric, exchange matrix,

$$R_d^3 = k_d^3 K_d^3 = k_d^3 \frac{1}{2} \begin{pmatrix} -2 & 1 & 1 & 0 & 0 & 0 & 0 \\ 1 & -2 & 0 & 0 & 1 & 0 & 0 \\ 1 & 0 & -2 & 0 & 0 & 1 & 0 \\ 0 & 0 & 0 & 0 & 0 & 0 & 0 \\ 0 & 1 & 0 & 0 & -2 & 1 & 0 \\ 0 & 0 & 1 & 0 & 1 & -2 & 0 \\ 0 & 0 & 0 & 0 & 0 & 0 & 0 \end{pmatrix}, \quad [5]$$

where k_d^3 is the rate for any one of the two permutations. The subscript refers to "double bond shift" and the superscript to the wing in the P_7 cage that remains unaltered during this process.

In principle, one could imagine that the rearrangement is accompanied by a concomitant, or independent, threefold molecular reorientation, as found in bullvalene (*12*,*17*). However, as will be shown in the next section, such reorientations do not seem to occur, at least not at rates sufficiently fast to affect the dynamic lineshapes, and we therefore do not include them in the analysis. The four other double bond-shift pathways can readily be written down as the cyclic permutations of the phosphorus atoms in the two other five rings, and their inverses,

$$(3B, 3E, A, 1E, 1B)(2B)(2E)$$
$$(3B, 1B, 1E, A, 3E)(2B)(2E)$$

and

$$(2B, 2E, A, 3E, 3B)(1B)(1E)$$
$$(2B, 3B, 3E, A, 2E)(1B)(1E).$$

The resulting exchange matrices for these two additional pairs of permutations then become

$$R_d^2 = k_d^2 K_d^2 = k_d^2 \frac{1}{2} \begin{pmatrix} -2 & 1 & 0 & 1 & 0 & 0 & 0 \\ 1 & -2 & 0 & 0 & 1 & 0 & 0 \\ 0 & 0 & 0 & 0 & 0 & 0 & 0 \\ 1 & 0 & 0 & -2 & 0 & 0 & 1 \\ 0 & 1 & 0 & 0 & -2 & 0 & 1 \\ 0 & 0 & 0 & 0 & 0 & 0 & 0 \\ 0 & 0 & 0 & 1 & 1 & 0 & -2 \end{pmatrix} \quad [6]$$

and

$$R_d^1 = k_d^1 K_d^1 = k_d^1 \frac{1}{2} \begin{pmatrix} -2 & 0 & 1 & 1 & 0 & 0 & 0 \\ 0 & 0 & 0 & 0 & 0 & 0 & 0 \\ 1 & 0 & -2 & 0 & 0 & 1 & 0 \\ 1 & 0 & 0 & -2 & 0 & 0 & 1 \\ 0 & 0 & 0 & 0 & 0 & 0 & 0 \\ 0 & 0 & 1 & 0 & 0 & -2 & 1 \\ 0 & 0 & 0 & 1 & 0 & 1 & -2 \end{pmatrix}. \quad [7]$$

If we now assume that all pathways have the same rates, $k_d^1 = k_d^2 = k_d^3$, the following overall exchange matrix is obtained,

$$R_d = R_d^1 + R_d^2 + R_d^3 = k_d K_d$$
$$= k_d \frac{1}{6} \begin{pmatrix} -6 & 2 & 2 & 2 & 0 & 0 & 0 \\ 2 & -4 & 0 & 0 & 2 & 0 & 0 \\ 2 & 0 & -4 & 0 & 0 & 2 & 0 \\ 2 & 0 & 0 & -4 & 0 & 0 & 2 \\ 0 & 2 & 0 & 0 & -4 & 1 & 1 \\ 0 & 0 & 2 & 0 & 1 & -4 & 1 \\ 0 & 0 & 0 & 2 & 1 & 1 & -4 \end{pmatrix}, \quad [8]$$

where $k_d = 3k_d^i$ ($i = 1-3$) is now the rate that any one of the six possible permutations take place and $K_d = \frac{1}{3}(K_d^1 + K_d^2 + K_d^3)$. To facilitate the comparison with the 2D exchange spectrum we contract this exchange matrix, by grouping together sites belonging to the same type of phosphorus atoms. The result is

$$R_d^* = k_d K_d^* = k_d \begin{pmatrix} -1 & \frac{1}{3} & 0 \\ 1 & -\frac{2}{3} & \frac{1}{3} \\ 0 & \frac{1}{3} & -\frac{1}{3} \end{pmatrix}, \qquad [9]$$

where, as for the R_s^* matrix, the rows and columns are labeled in the order A, E, B. For short mixing times, this exchange matrix predicts cross peaks within the pairs A/E and E/B, but no such peaks between A and B. This is exactly the pattern of cross peaks observed experimentally in the 2D exchange spectrum of Fig. 4. On the left hand side of the figure is shown a simulated 2D spectrum calculated using Eq. [8] for $k_d\tau = 1$, showing a pattern very similar to the experimental one on the right. This strongly suggests that double bond shift is indeed the mechanism responsible for the dynamic line broadening observed in the MAS spectra of solid $Li_3P_7(mg)_3$. To check whether this mechanism indeed yields simulated 1D spectra that are consistent with the experimental results, we first assumed that all three pairs of permutations have equal rates, $k_d^1 = k_d^2 = k_d^3 = k_d$, and accordingly used Eq. [8] for the simulations. Results so obtained for different k_d values are shown in the middle column of Fig. 3. The fit with the experimental spectra (left column) is now much improved in comparison with the single bond-shift mechanism (right column). In particular, we note that the relative broadening of the E and B bands is quite similar to that observed experimentally. In fact, the similarity between the calculated and experimental spectra is satisfactory enough to derive good estimates for the kinetic parameters of the reaction. Performing such an analysis yields the following average Arrhenius parameters, $E_a \sim 50$ kJ/mol and $k_d(17^\circ\text{C}) \sim 2 \times 10^4\ \text{s}^{-1}$. However, the k_d vs $1/T$ plot, so obtained, is not a straight line but rather curved, with slopes ranging from 30 kJ/mol at low temperatures to 70 kJ/mol at high temperatures. This and the fact that the low-temperature spectra are not perfectly reproduced by the simulations indicate that the situation is somewhat more complicated. We discuss this issue in the next section.

3.4. The Effect of the Cage Asymmetry

Close inspection of the spectra in Fig. 3, particularly, at low temperatures where the triplet structure of the E band is still partially resolved, reveals delicate differences between the experimental (left column) and simulated (middle column) lineshapes. It may be seen that in the experimental spectra the three E lines do not broaden to the same extent as they do in the simulation. We recall that the exchange matrix R_d (Eq. [8]), used in the simulation, represents the sum of three pairs of processes with equal rates, each involving a cyclic permutation of atoms within one of the three five-rings in the P_7 cage. For a particular five-ring permutation, R_d^i, two atoms, iE and iB, are not involved in the exchange and therefore their NMR peaks remain unaffected by the rearrangement process. Referring to the low-temperature spectra in Figs. 2 and 3, we note that while the lines labeled 2E and 3E start to broaden already at -60°C, line 1E remains sharp up to well above -10°C. This clearly indicates that the three processes represented by R_d^1, R_d^2, and R_d^3, Eqs. [5]–[7], do not have the same rate parameters, as assumed in the simulations of the center column of Fig. 3. This is perhaps not surprising in view of the fact that the P_7 cage in solid $Li_3P_7(mg)_3$ lacks exact threefold symmetry, as we have seen in the low-temperature spectra (Fig. 2). From the experimental spectra it is thus clear that at low temperatures ($<\sim 10^\circ$C) k_d^2 and k_d^3, which lead to broadening of the 1E line, are considerably smaller than k_d^1, which does not affect the width of this peak, but does affect the 2E and 3E lines.

For the final simulations of the spectra we have therefore used the exchange matrix

$$R_d = k_d^1 K_d^1 + k_d^2 K_d^2 + k_d^3 K_d^3 \qquad [10]$$

with, in general, different rate constants for the different permutations. Since, however, the broadening of the 2E and 3E lines appears to be quite similar, and to simplify the fitting procedure, we assumed that $k_d^2 = k_d^3$ and took k_d^1 and $k_d^{23} (= k_d^2 = k_d^3)$ as adjustable parameters in the fitting procedure. In Fig. 5 are shown experimental spectra on a more finely spaced temperature scale than in Fig. 3, together with our best fit simulations to Eq. [10]. The fit is now considerably improved and particularly reproduces well the dynamic lineshape of the E band. These results confirm that at low temperatures the dominant process is indeed R_d^1, while at higher temperatures the two other processes take over. The results also show that, at least at low temperatures, no threefold molecular jumps take place. Otherwise the 1E line would also broaden. Such threefold jumps are quite common for globular molecules with C_{3v} symmetry like bullvalene (*12*) and certain phosphorus cage compounds (*21*), but apparently they do not occur in $Li_3P_7(mg)_3$. An overall analysis of the experimental spectra, using Eq. [10] and the parameters of Table 1, yielded the Arrhenius plots shown in Fig. 6. The kinetic parameters derived from these results are summarized in Table 2. Note that to optimize the fit, in particular at low temperatures, we had to introduce some temperature dependence in δ_{iso}, as indicated in Table 1. These are very small shifts and chemically not unrealistic.

Admittedly, the fit of the 1D dynamic spectra in Fig. 5 is still not perfect. For example, the temperature range -20 to -40°C the relative intensities of the B and E peaks differ in the experimental and simulated spectra. We were unable to improve the fit using the parameters of Table 1. It is possible that this disagreement is due to an error in the orientation of the principal directions of the chemical shift tensors of the E and B nuclei. These were determined in I by quantum mechanical calculations and we have no way to assess their accuracy. Also the assignment

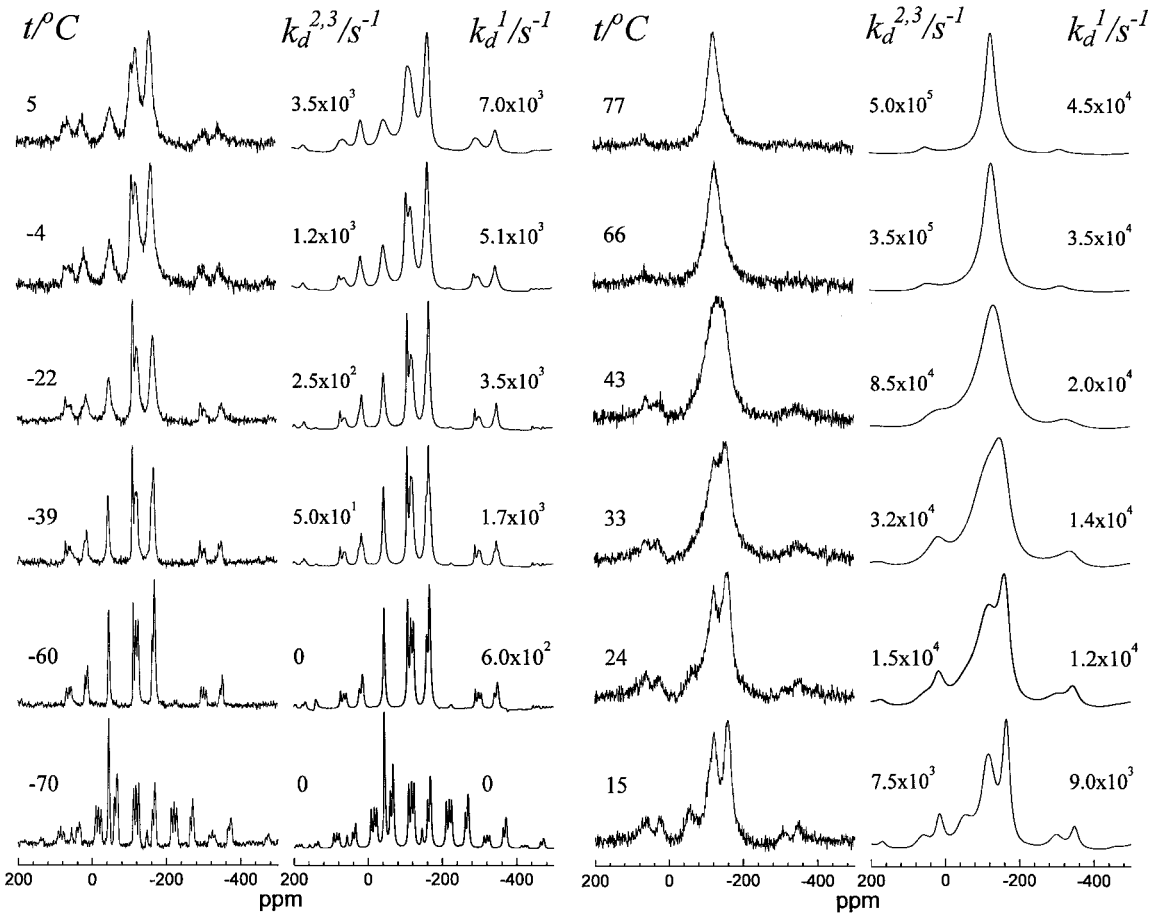

FIG. 5. More detailed dynamic ^{31}P MAS NMR spectra of solid $Li_3P_7(mg)_3$. First and third columns: Experimental spectra as a function of the indicated temperatures. The experimental details are as in the caption to Fig. 3, except that the $-70°C$ spectrum was recorded at a spinning rate of 16.4 kHz with a recycle time of 240 s. Second and fourth columns: Simulated spectra for the double bond-shift mechanism, assuming $k_d^1 \neq k_d^2 = k_d^3 = k_d^{2,3}$ and the indicated k_d^i values (Eqs. [10] and [5]–[7]).

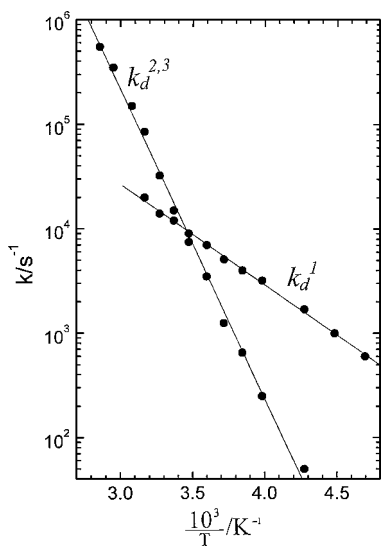

FIG. 6. Arrhenius plots of the double bond-shift processes, k_d^1 and $k_d^{2,3}(=k_d^2=k_d^3)$ in solid $Li_3P_7(mg)_3$, as derived from dynamic MAS spectra of the type shown in Fig. 5.

of the B peaks (Table 1) is somewhat uncertain. It was done by fitting the low temperature dynamic spectra to the simulations. This fitting showed that the 1B peak (which remains sharp at low temperatures) must be part of the more intense component of the B doublet (see Fig. 2), but the exact chemical shifts of the B lines is certainly not as accurately determined as for the E lines.

TABLE 2
Kinetic Data for the Bond-Shift Rearrangement in Solid $Li_3P_7(mg)_3$ and in Solution[a]

	$k(17°C)/s^{-1}$	E_a/kjmol^{-1}
k_d^1	10^4	18.7
$k_d^{2,3}$	10^4	58.0
k_s(solution)	0.7×10^4	46 − 63

[a] The results for k_d^1 and $k_d^{2,3}(=k_d^2=k_d^3)$ in the solid state are from the present work. The results for k(solution) were derived from data given in Baudler *et al.* (*5*) using the exchange matrix shown in Eq. [4].

4. SUMMARY AND CONCLUSIONS

We have studied the ^{31}P MAS NMR spectrum of solid $Li_3P_7(mg)_3$ over a wide temperature range. The results provide detailed information regarding the structural and dynamic properties of the P_7 cage in this solid. The low-temperature NMR spectra are consistent with the P_7-cage structure shown in Fig. 1, with a small distortion from perfect C_{3v} symmetry. The distortion is clearly reflected in the triplet splitting of the E signal and the unresolved structure of the B band. This result is consistent with the X-ray structure of the homologous compound, $Li_3P_7(tmeda)_3$, where the P_7 cage was found to have nearly, but not perfect C_{3v} symmetry (*4*).

The MAS NMR spectra are strongly temperature dependent, reflecting the bond-shift rearrangement of the P_7 cage. In I, an attempt was made to quantitatively analyze such dynamic NMR spectra in terms of a concerted process (Scheme B), involving chemical bond shift and an overall molecular reorientation that ensures the preservation of the lattice order—a bond shift alone would result in an inverted cage and thus in a disordered lattice. A concerted bond-shift/reorientation mechanism was proven to occur in the analogous situation of the Cope rearrangement in solid bullvalene (*11, 12, 17*). However, for the case of $Li_3P_7(mg)_3$ such a dynamic model did not give a satisfactory fit to the experimental spectra. Instead, we have now shown that the rearrangement in solid $Li_3P_7(mg)_3$ proceeds by a quite different route, involving a double bond shift (Scheme C). The reason for the different pathways in the two systems most likely lies in the fact that the bullvalene molecule is neutral and as the bond-shift reaction proceeds a "soft" transition intermediate is obtained that can readily slip to the desired orientation in the lattice. On the other hand, the P_7 cage with its negatively charged equatorial atoms is held by a belt of positively charged Li cations, which are fixed in the lattice. As the bond shift takes place, negative charges move from two equatorial to the neighboring basal atoms, interchanging their chemical nature. The cage is now inverted and still held by the same Li^+ belt. It is therefore under strain, but cannot easily reorient. Instead, it undergoes a second bond shift that restores its proper orientation in the lattice and relieves the strain. The second rearrangement can involve one of the three bonds of the newly formed basal P-P-P triangle. If it happens to be the same bond as the one just formed, no net permutation of atoms takes place. However, a reverse bond shift involving one of the other two bonds does result in a permutation. Hence, assuming statistical likelihood for the three alternatives, the rate of formation of the intermediate species by the first bond shift is, in fact, a factor of 1.5 faster than given in Table 2.

As we have seen, the double bond-shift process actually amounts to a cyclic permutation of the phosphorus atoms around the five rings of the P_7 cage, i.e., in a very small displacement of the cage atoms, of the order of a P–P bond length. The situation is similar to that found for the analogous rearrangement in some monosubstituted bullvalenes (*22–24*) as, for example, fluoro- or cyano-bullvalene. These compounds too were found to undergo Cope rearrangement in the solid state by a multiple bond-shift mechanism, depending on the substitution site, that ensured the preservation of the crystal order. Exceptions to this rule are bromo-, iodo-, and possibly chlorobullvalene (25), which form disordered crystals. In these cases orientational order need not be preserved and single bond-shift pathways are allowed, and indeed were found to occur.

The deviation of the P_7- cage structure from perfect C_{3v} symmetry in the solid state is also reflected in its fluxional properties. In particular, we found that the rates of the cyclic permutations are not equal for the three five-rings. As it turned out there is one five-ring that, at low temperatures, is more labile than its two neighbors. It is interesting to mention that even for unsubstituted bullvalene, different rates for the different single bond-shift pathways were found in the solid state (*17*), apparently caused by the nonsymmetric environment in the crystal. Finally, we mention the somewhat surprising result that, over the entire temperature range studied, the rearrangement rate in the solid is faster than in solution (see Table 2).

The detailed structural and dynamic information obtained on the $Li_3P_7(mg)_3$ system in the present work demonstrates the power of 1D and 2D dynamic ^{31}P MAS NMR in the study of solids. It also demonstrates the wealth of motional processes that may take place in what we often think to be rigid solids.

ACKNOWLEDGMENTS

This work was supported by the German–Israeli Foundation, G.I.F. Project I-558.218.05/97 and by the Deutsche Forschungsgemeinschaft (SFB 418). We thank the support of Horst Schneider (Halle) and the fonds der Chemischen Industrie. We are also indebted to Stephanie Hesse (Jena) for the help in painstakingly packing the sample in the glovebox for the NMR measurements.

REFERENCES

1. T. Sen, R. Poupko, U. Fleischer, H. Zimmermann, and Z. Luz, *J. Am. Chem. Soc.* **122,** 889 (2000).
2. M. Baudler and K. Glinka, *Chem. Rev.* **93,** 1623 (1993).
3. M. Baudler, *Angew. Chem. Int. Ed. Engl.* **21,** 492 (1982).
4. W. Hönle, H. G. von Schnering, A. Schmidpeter, and G. Burget, *Angew. Chem. Int. Ed. Engl.* **23,** 817 (1984).
5. M. Baudler, H. Ternberger, W. Faber, and J. Hahn, *Z. Naturforsch. B* **34,** 1690 (1979).
6. M. Baudler, Th. Pontzen, J. Hahn, H. Ternberger, and W. Faber, *Z. Naturforsch. B* **35,** 517 (1980).
7. M. Baudler and J. Hahn, *Z. Naturforsch. B* **45,** 1279 (1990).
8. R. K. Harris and A. C. Olivieri, *Prog. NMR Spectros.* **24,** 435 (1992).
9. J. F. M. Oth, K. Müllen, J.-M. Gilles, and G. Schröder, *Helv. Chim. Acta* **57,** 1415 (1974).
10. B. H. Meier and W. L. Earl, *J. Am. Chem. Soc.* **107,** 5553 (1985).
11. J. J. Titman, Z. Luz, and H. W. Spiess, *J. Am. Chem. Soc.* **114,** 3765 (1992).
12. S. Schlick, Z. Luz, R. Poupko, and H. Zimmermann, *J. Am. Chem. Soc.* **114,** 4315 (1992).
13. A. Bielecki and D. P. Burum, *J. Magn. Reson. A* **116,** 215 (1995).

14. A. Schmidt and S. Vega, *J. Chem. Phys.* **87,** 6895 (1987).
15. Z. Luz, R. Poupko, and S. Alexander, *J. Chem. Phys.* **99,** 7544 (1993).
16. J. Herzfeld and A. E. Berger. *J. Chem. Phys.* **73,** 6029 (1980).
17. A. Müller, U. Haeberlen, H. Zimmermann, R. Poupko, and Z. Luz, *Mol. Phys.* **81,** 1239 (1994).
18. A. F. de Jong, A. P. M. Kentgens, and W. S. Veeman, *Chem. Phys. Lett.* **109,** 337 (1984).
19. M. Hamermesh, "Group Theory," p. 13, Pergamon, London (1962).
20. R. C. Tolman, "The Principles of Statistical Mechanics," p. 163, Oxford Univ. Press, London (1938).
21. W. Hoffbauer, S. Weffing, G. Klösters, F. Frick, and M. Jansen, *Solid State Nucl. Magn. Reson.* **14,** 211 (1999).
22. K. Müller, H. Zimmermann, C. Krieger, R. Poupko, and Z. Luz, *J. Am. Chem. Soc.* **118,** 8006 (1996).
23. R. Poupko, K. Müller, C. Krieger, H. Zimmermann, and Z. Luz, *J. Am. Chem. Soc.* **118,** 8015 (1996).
24. L. Olivier, R. Poupko, H. Zimmermann, and Z. Luz, *J. Phys. Chem.* **100,** 17995 (1996).
25. Z. Luz, L. Oliver, R. Poupko, K. Müller, C. Krieger, and H. Zimmermann, *J. Am. Chem. Soc.* **120,** 5526 (1998).